

Selective separation of *meta*- and *para*-cresol using nonporous adaptive crystals of perpropoxylated pillar[5]arene

Hongyan Zhang,^a Ming Li,^{*a} Li Shao,^c Haozhong Liang,^a Bin Hua,^{*a,b} Niveen M. Khashab^{*d} and Feihe Huang^{*a,b}

^a*Stoddart Institute of Molecular Science, Department of Chemistry, Zhejiang University, Hangzhou 310058, P. R. China; Fax and Tel: +86-571-8795-3189*

^b*Zhejiang-Israel Joint Laboratory of Self-Assembling Functional Materials, ZJU-Hangzhou Global Scientific and Technological Innovation Center, Zhejiang University, Hangzhou 311215, P. R. China*

^c*Department of Materials Science and Engineering, Zhejiang Sci-Tech University, Hangzhou 310018, P. R. China*

^d*Smart Hybrid Materials Laboratory (SHMs), Department of Chemistry, Division of Physical Science and Engineering, King Abdullah University of Science and Technology (KAUST), Thuwal 23955-6900, Kingdom of Saudi Arabia.*

Email addresses: mingzhelee@zju.edu.cn; huabin@zju.edu.cn; niveen.khashab@kaust.edu.sa; fhuang@zju.edu.cn.

Electronic Supplementary Information

1. <i>Materials and methods</i>	S2
2. <i>Synthesis of the host PrP5</i>	S4
3. <i>Investigation of host–guest complexation behavior in solution</i>	S5
4. <i>X-ray crystal data of (MC)₂@PrP5</i>	S7
5. <i>Theoretical calculations</i>	S9
6. <i>Studies of selective adsorption behavior of PrP5 solids</i>	S12
7. <i>Studies of selective adsorption behavior of EtP5 and BuP5 solids</i>	S20
8. <i>Studies of selective adsorption behavior of PrP5@MSN-OH solids</i>	S24
9. <i>References</i>	S26

1. Materials and methods

Materials

All reagents including guest compounds were commercially available and used as supplied without further purification. Solvents were either employed as purchased or dried according to procedures described in the literature. Compound **PrP5** was prepared according to a published procedure.^{S1,S2}

Methods

¹H NMR: NMR spectra were recorded with a Bruker Avance DMX 400 spectrophotometer or a Bruker Avance DMX 500 spectrophotometer using the deuterated solvent as the lock and the residual solvent or TMS as the internal reference.

Thermogravimetric analysis: TGA was carried out using a Q5000IR analyzer (TA Instruments) with an automated vertical overhead thermo balance. The samples were heated at 10 °C/min using N₂ as the protective gas.

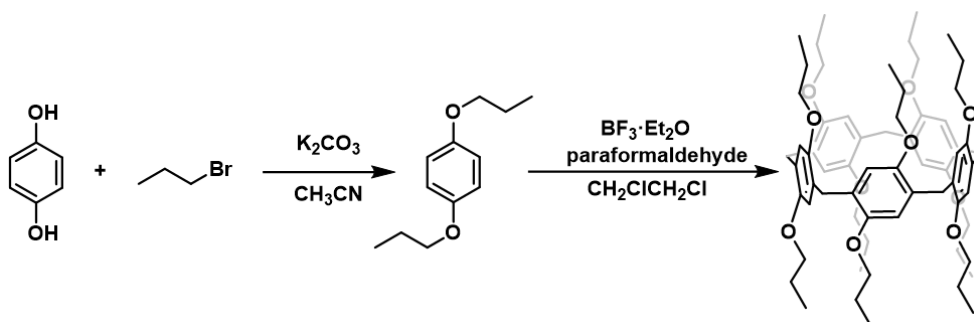
X-ray powder diffraction: PXRD data were measured on a SmartLab diffractometer with fixed divergence slits and a D/tex Ultra 250 detector at room temperature. The diffractometer was configured in parafocusing Bragg-Brentano geometry. Data was collected over a 2θ range of 5° to 45° with a step size of 0.02° and a scan rate of 5°/min using a Cu K_{α} radiation at a powder of 40 kV and 180 mA. Cu K_{β} radiation was removed using a divergent beam Ni filter.

Single crystal X-ray diffraction: SCXRD data were collected on a Bruker D8 VENTURECMOS X-ray diffractometer with graphite monochromatic Mo- K_{α} radiation ($\lambda = 0.71073 \text{ \AA}$).

Gas chromatographic analysis: GC analysis measurements were carried out using an Agilent 7890B instrument configured with an FID detector and a HP-chiral β column (30 m \times 0.32 mm \times 0.25 μ m). Samples were analyzed using direct injection. The instrument was set with the inlet temperature at 200 °C, a split ratio of 20 : 1, a flow rate of 1.5 mL/min and the detector temperature at 200 °C. 1 μ L of the sample was injected and the temperature program included maintaining at 60 °C for 3 minutes, heating up to 200 °C at a rate of 20 °C/min, and keeping at 200 °C for 3 minutes.

Independent gradient model calculations: The calculated structure was built from the single crystal structure of **(MC)₂@PrP5**. All-electron DFT calculations were carried out using the ORCA quantum chemistry software (Version 5.0.3).^{S3} The positions of the hydrogen atoms were optimized, and the other atoms were maintained unchanged in their respective positions. The B3LYP functional^{S4} and 6-31g(d) basis set^{S5} were employed for the DFT structural optimization calculations. DFT-D3 with BJ-damping^{S6} was applied to correct for weak interactions and improve the calculation accuracy. The nature of noncovalent interactions was studied by using the IGMH (Independent gradient model based on Hirshfeld partition) method^{S7} through Multiwfn software.^{S8} The visualization of IGMH were rendered by VMD.^{S9}

2. Synthesis of the host **PrP5**



Scheme S1 Synthetic route to **PrP5**.

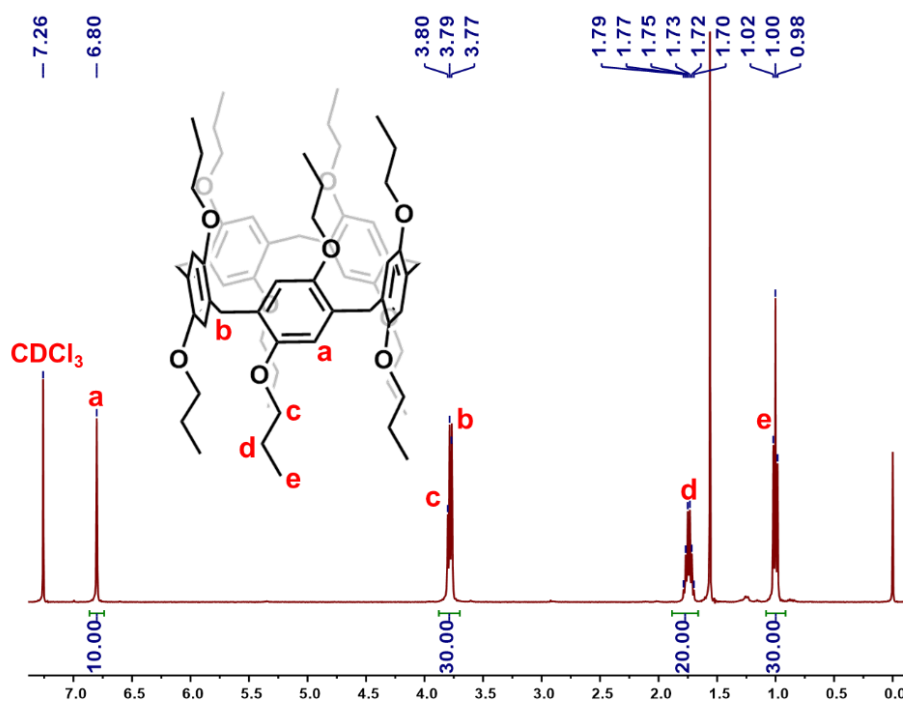


Fig. S1 1H NMR spectrum (500 MHz, $CDCl_3$, room temperature) of **PrP5**.

3. Investigation of host-guest complexation behavior in solution

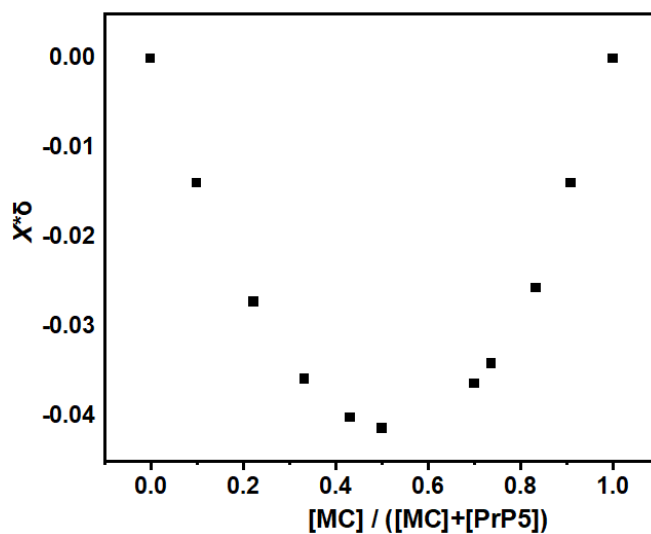


Fig. S2 Job plot showing the 1 : 1 stoichiometry of the complexation between **PrP5** and **MC** in CDCl_3 .

Based on ^1H NMR spectroscopic results, a Job plot was created to study the binding stoichiometry between **PrP5** and **MC**. The total concentration of [**P5**] and [**MC**] was set at 10.00 mM. The minimum peak is corresponding to the value of 0.50 ($[\text{MC}]/([\text{PrP5}]+[\text{MC}])$) for the mole fraction X of the guest **MC**, a finding consistent with a 1 : 1 (**PrP5** : **MC**) binding stoichiometry.

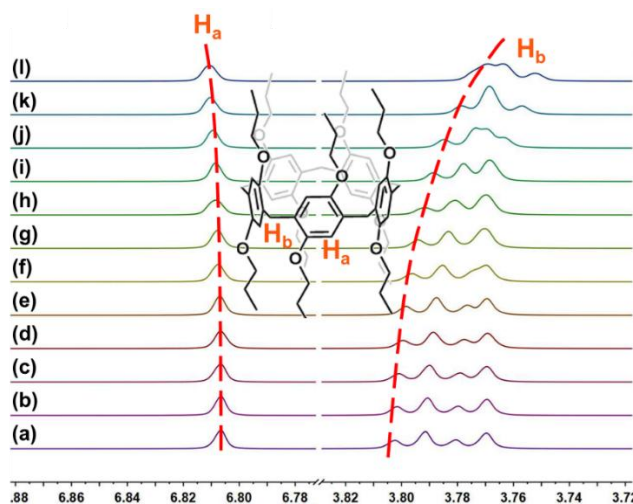


Fig. S3 Partial ^1H NMR spectra (600 MHz, CDCl_3 , room temperature) of **PrP5** at a constant concentration of 10.00 mM upon gradual addition of **MC**. The concentrations of **MC** in solutions: (a) 0.00 mM; (b) 1.00 mM; (c) 1.96 mM; (d) 3.85 mM; (e) 5.66 mM; (f) 9.09 mM; (g) 12.28 mM; (h) 15.97 mM; (i) 20.00 mM; (j) 25.93 mM; (k) 35.48 mM; (l) 42.86 mM.



Fig. S4 A plot of the resonance field shifts of H_a and H_b of **PrP5** with respect to the molar ratio of [MC]/[PrP5]. The data were fitted to a 1 : 1 binding model, yielding $K_a = (2.78 \pm 0.03) \text{ M}^{-1}$. The solid lines on the graph were obtained through non-linear curve-fitting using the web applet available at app.supramolecular.org/bindfit/.

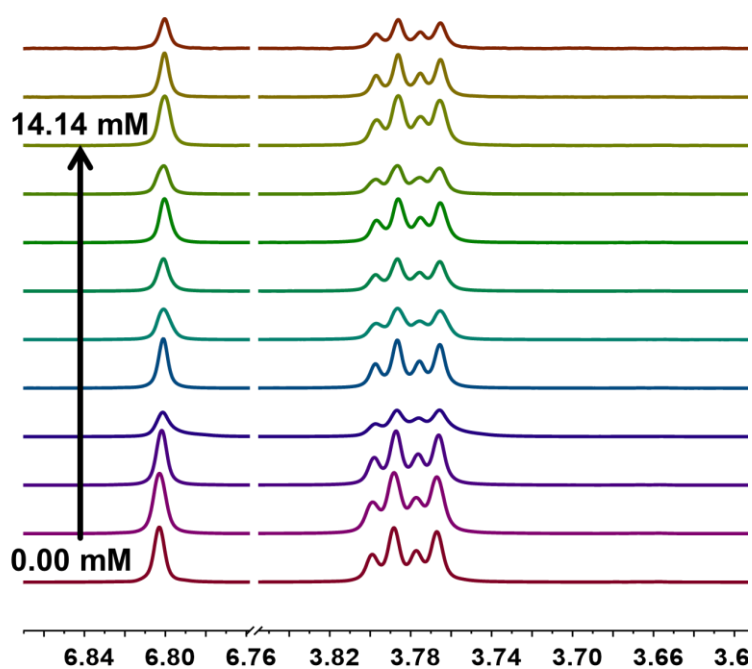


Fig. S5 Partial ¹H NMR spectra (600 MHz, CDCl₃, room temperature) of **PrP5** at a constant concentration of 1.00 mM upon gradual addition of **PC**. The concentrations of **PC** in solution ranged from 0.00 mM to 14.14 mM.

4. X-ray crystal data of (MC)₂@PrP5

Crystals were obtained by slow diffusion of MeOH into a mixed solution containing **PrP5** and **MC**. In the single crystal structure of (MC)₂@PrP5, the molar ratio of **PrP5** and **MC** in the resulting host–guest complex crystal structure was 1 : 2. CCDC number: 2423863.

Table S1 Experimental crystallographic data for (MC)₂@PrP5.

Parameters	(MC) ₂ @PrP5
Formula	C ₇₉ H ₁₀₆ O ₁₂
<i>FW</i>	1247.63
Temp. (K)	170.00
Crystal system	Triclinic
Space group	<i>P</i> $\bar{1}$
<i>a</i> (Å)	12.1416(5)
<i>b</i> (Å)	14.7670(6)
<i>c</i> (Å)	21.8610(9)
α (°)	91.6110(10)
β (°)	95.3400(10)
γ (°)	111.9970(10)
<i>Volume</i> (Å ³)	3610.0(3)
<i>Z</i>	2
ρ_{calc} (g cm ⁻³)	1.148
<i>F</i> (000)	1352.0
Independent reflections	16368 [<i>R</i> _{int} = 0.0433]
Goodness-of-fit on <i>F</i> ²	1.066
Final <i>R</i> indexes [<i>I</i> ≥ 2σ(<i>I</i>)]	<i>R</i> ₁ = 0.0509, <i>wR</i> ₂ = 0.1357
Final <i>R</i> indexes [all data]	<i>R</i> ₁ = 0.0610, <i>wR</i> ₂ = 0.1440
Largest diff. peak/hole (e Å ⁻³)	0.64/−0.40

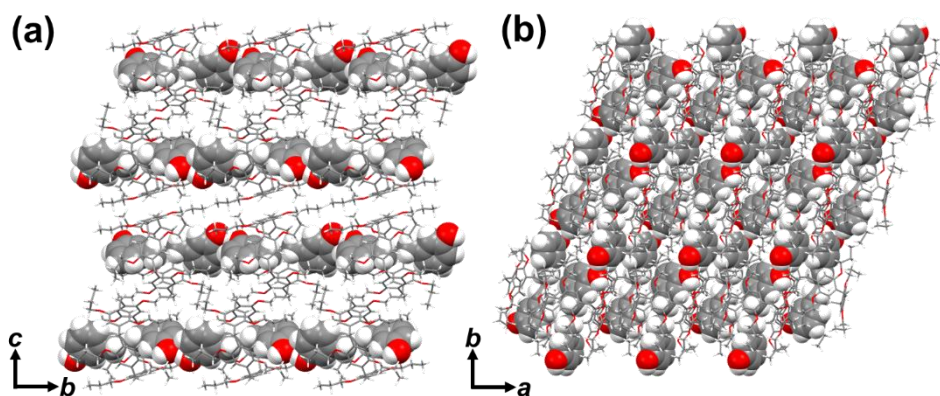


Fig. S6 Different views of the single crystal structure of $(MC)_2@PrP5$: (a) along the a -axis; (b) along the c -axis.

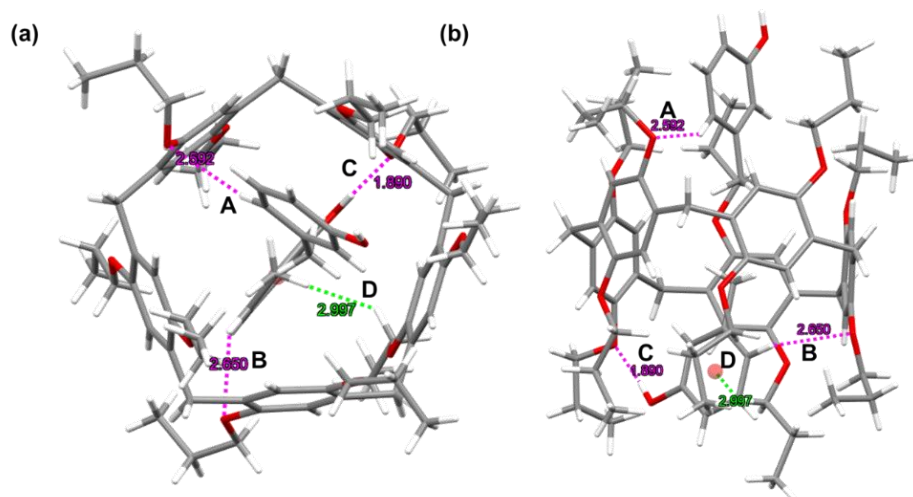


Fig. S7 Illustration of non-covalent interactions: (a) top view; (b) side view. C–H \cdots O distances (Å) and C–H \cdots O angles (degrees): **A**, 2.59, 145.18; **B**, 2.65, 146.43. O–H \cdots O distance (Å) and O–H \cdots O angle (degree): **C**, 1.89, 174.69. C–H \cdots π plane distance (Å) and C–H \cdots π angle (degree): **D**, 3.00, 132.38.

5. Theoretical calculations

All-electron DFT calculations have been carried out by the ORCA quantum chemistry software (Version 6.0.0). The BLYP functional and def2-SVP basis set were adopted for geometry optimization and frequency calculations, and the optimal geometry for each compound was determined. The single point energy calculations were performed with B3LYP functional and a larger basis set def2-TZVPD basis set. The DFT-D3 dispersion correction with BJ-damping was applied to correct the weak interactions to improve the calculation accuracy. IGMH analysis and ESP analysis were performed by Multiwfn software.

For **PrP5-PC** and **PrP5-MC** systems, due to uncertainty regarding whether the binding occurs in a 1 : 1 or 1 : 2 stoichiometry, we performed structural optimizations of **PC@PrP5**, **(PC)₂@PrP5**, **MC@PrP5** and **(MC)₂@PrP5** before computing the binding energies.

The binding energy (E_{BE}) values were calculated as follows:

For the 1 : 2 binding mode:

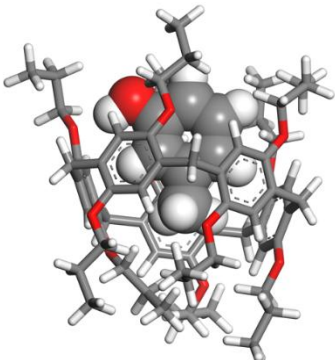
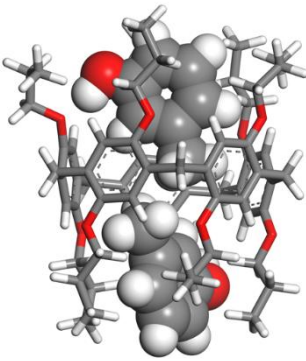
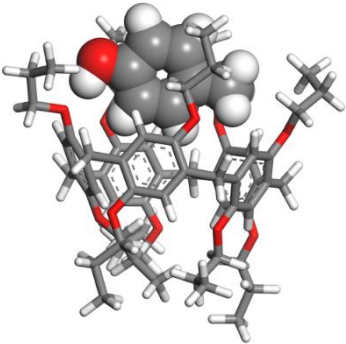
$$E_{BE} = E_{\text{complex}} - (E_{\text{PrP5}} + E_{\text{guest1}} + E_{\text{guest2}})$$

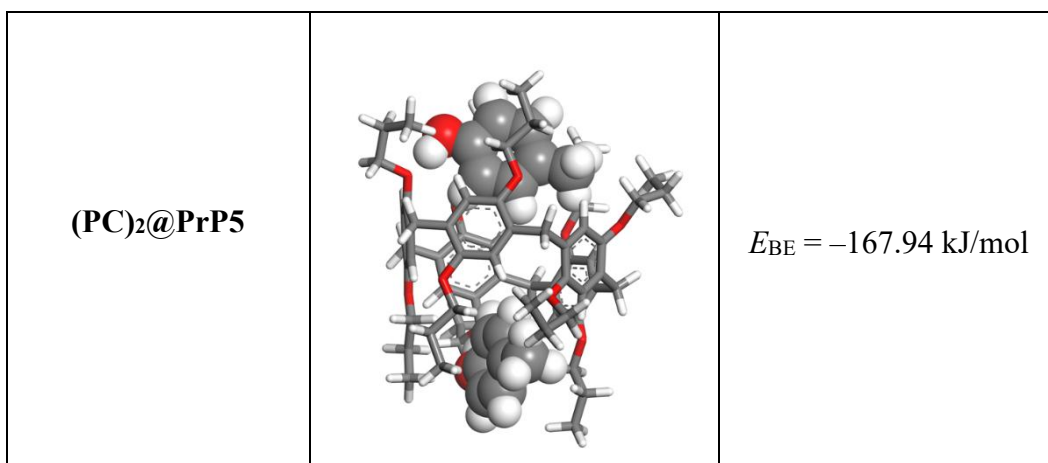
For the 1 : 1 binding mode:

$$E_{BE} = E_{\text{complex}} - (E_{\text{PrP5}} + E_{\text{guest}})$$

DFT calculations yielded binding energies of -131.55 kJ/mol for **MC@PrP5**, -225.89 kJ/mol for **(MC)₂@PrP5**, -92.35 kJ/mol for **PC@PrP5**, and -167.94 kJ/mol for **(PC)₂@PrP5**. These results clearly demonstrate that **(MC)₂@PrP5** exhibits the strongest binding energy among these four host–guest complexes. Therefore, **PrP5** showed the selective adsorption of **MC** over **PC** in the solid-gas adsorption experiments.

Table S2 Calculated structures of **MC@PrP5**, **(MC)₂@PrP5**, **PC@PrP5**, and **(PC)₂@PrP5** along with their binding energy.

Species	Calculated Structure	Binding Energy Value
MC@PrP5	 <p>A 3D ball-and-stick model of the MC@PrP5 complex. The structure shows a central metal atom (Pr) coordinated by a porphyrin-like ligand (P5) and a methylcyclopentadienyl (MC) group. The atoms are color-coded: carbon is grey, oxygen is red, and hydrogen is white.</p>	$E_{BE} = -131.55 \text{ kJ/mol}$
(MC)₂@PrP5	 <p>A 3D ball-and-stick model of the (MC)₂@PrP5 complex. The structure shows a central metal atom (Pr) coordinated by a porphyrin-like ligand (P5) and two methylcyclopentadienyl (MC) groups. The atoms are color-coded: carbon is grey, oxygen is red, and hydrogen is white.</p>	$E_{BE} = -225.89 \text{ kJ/mol}$
PC@PrP5	 <p>A 3D ball-and-stick model of the PC@PrP5 complex. The structure shows a central metal atom (Pr) coordinated by a porphyrin-like ligand (P5) and a pentamethylcyclopentadienyl (PC) group. The atoms are color-coded: carbon is grey, oxygen is red, and hydrogen is white.</p>	$E_{BE} = -92.35 \text{ kJ/mol}$



6. Studies of selective adsorption behavior of **PrP5** solids

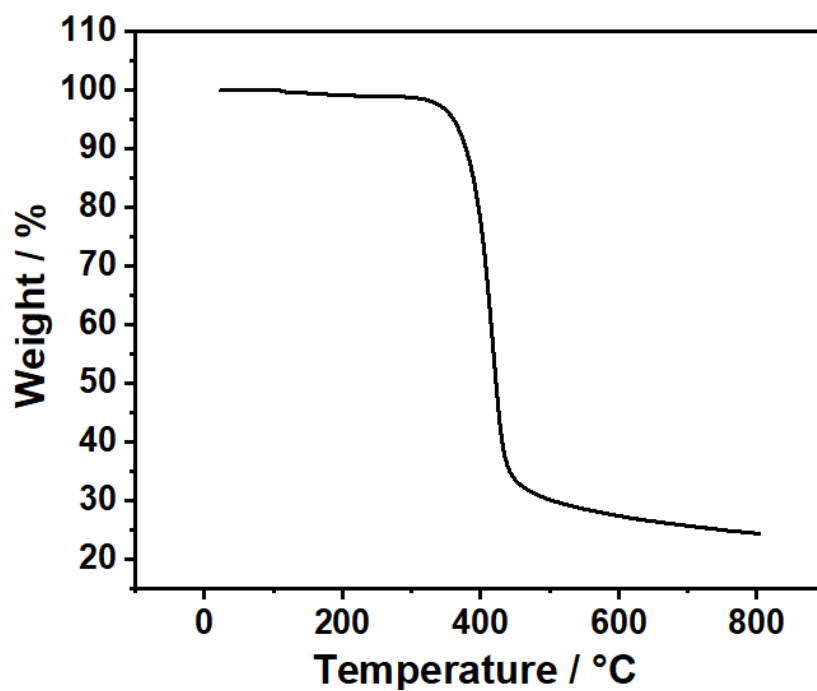


Fig. S8 Thermogravimetric analysis of **PrP5α**.

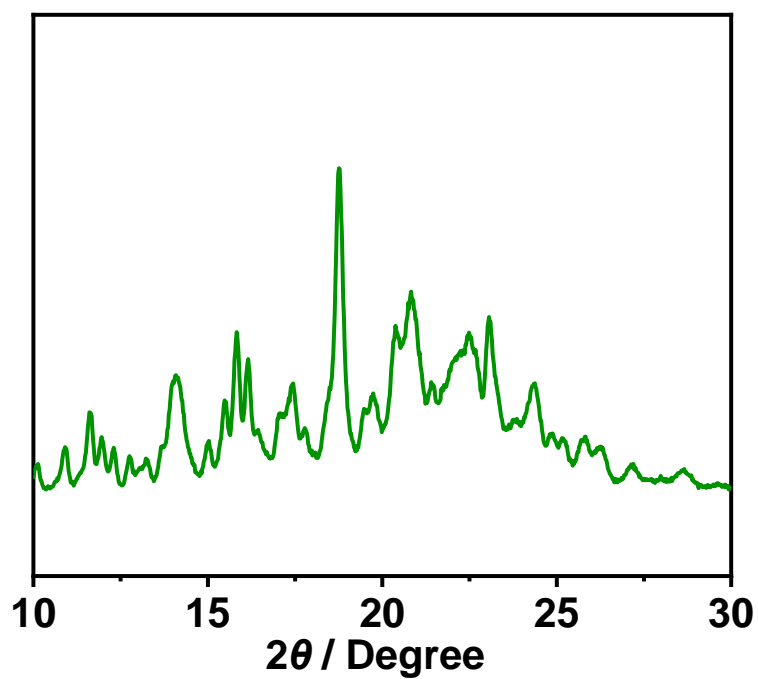


Fig. S9 Powder X-ray diffraction pattern of **PrP5α**.

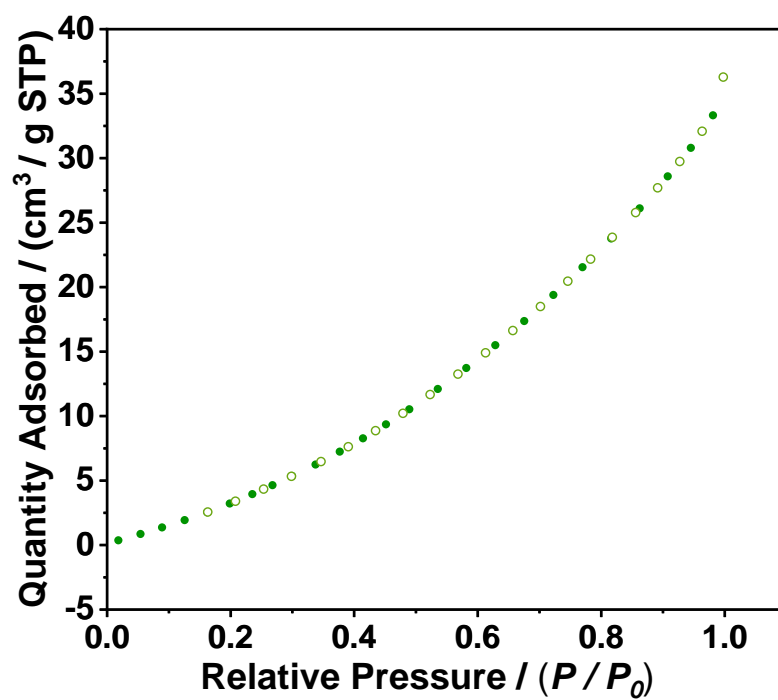


Fig. S10 N₂ adsorption isotherm of PrP5 α . The BET surface area value is 37.9 m² g⁻¹. Adsorption, solid symbols; desorption, open symbols.

Method: For each solid-vapor adsorption experiment, an open 5 mL vial containing 10 mg of the **PrP5 α** adsorbent was placed in a sealed 20 mL vial containing 1 mL of **MC**, **PC**, or a **MC/PC** mixture ($v : v = 1 : 1$).

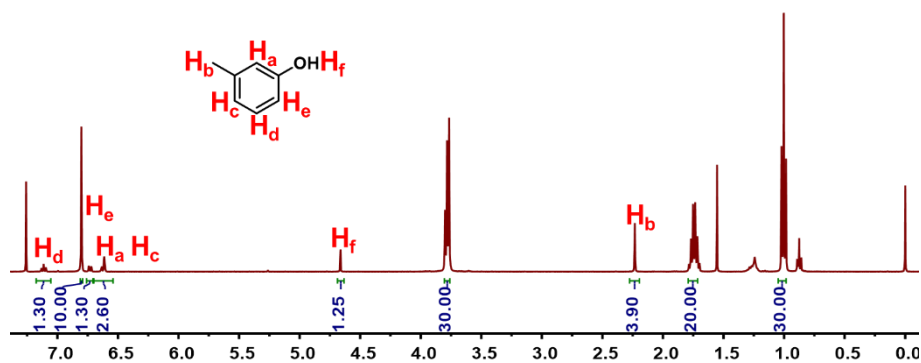


Fig. S11 ¹H NMR spectrum (400 MHz, CDCl₃, room temperature) of **PrP5 α** after being exposed to **MC** vapor for 48 h. Based on the integrated areas under these NMR peaks, approximate 1.30 equivalents of **MC** molecules were absorbed per **PrP5** molecule.

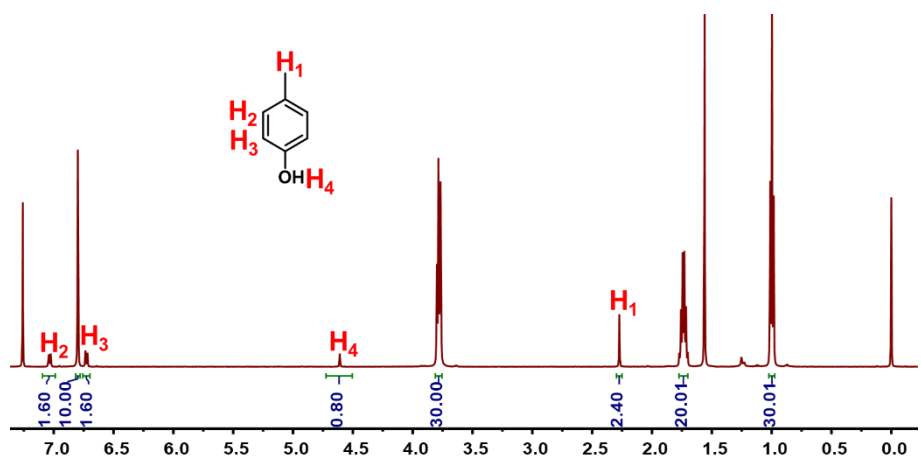


Fig. S12 ¹H NMR spectrum (400 MHz, CDCl₃, room temperature) of **PrP5 α** after being exposed to **PC** vapor for 48 h. Based on the integrated areas under these NMR peaks, approximate 0.80 equivalents of **PC** molecules were absorbed per **PrP5** molecule.

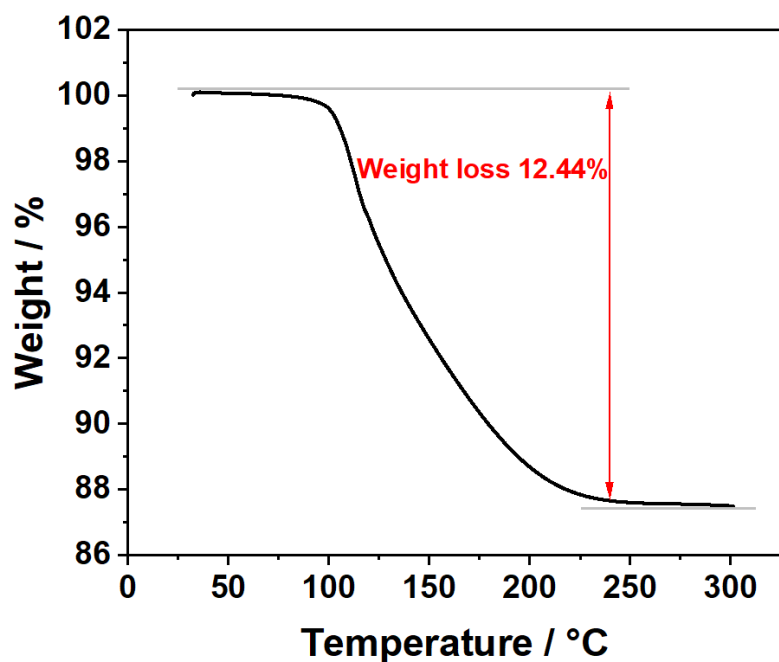


Fig. S13 Thermogravimetric analysis curve of **PrP5 α** after being exposed to **MC** vapor for 48 h. The weight loss corresponds to approximately 1.30 equivalents of **MC** molecules per **PrP5** molecule.

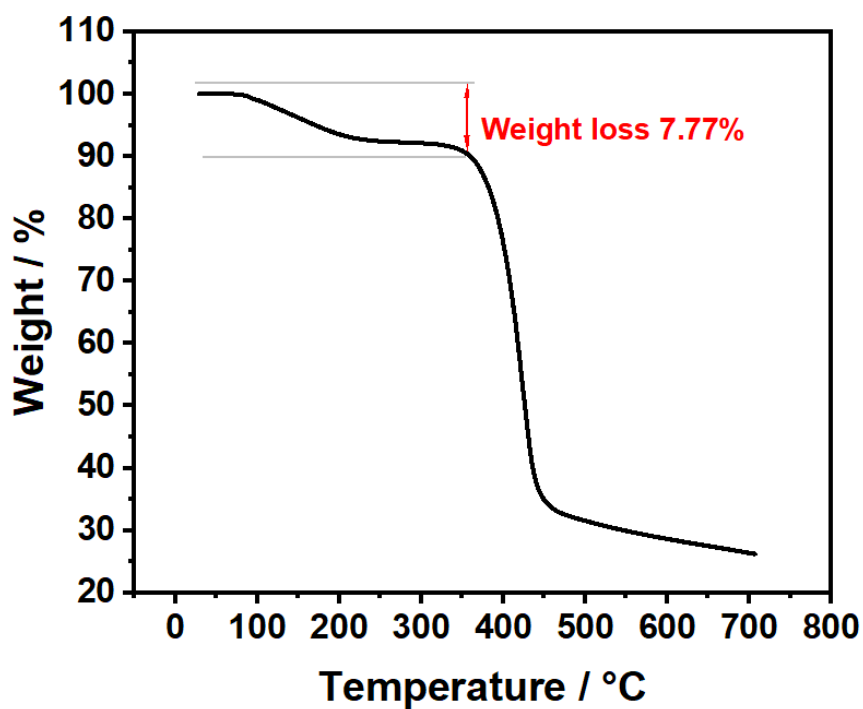


Fig. S14 Thermogravimetric analysis curve of **PrP5 α** after being exposed to **PC** vapor for 48 h. The weight loss below 350 °C corresponds to approximately 0.80 equivalents of **PC** molecules per **PrP5** molecule.

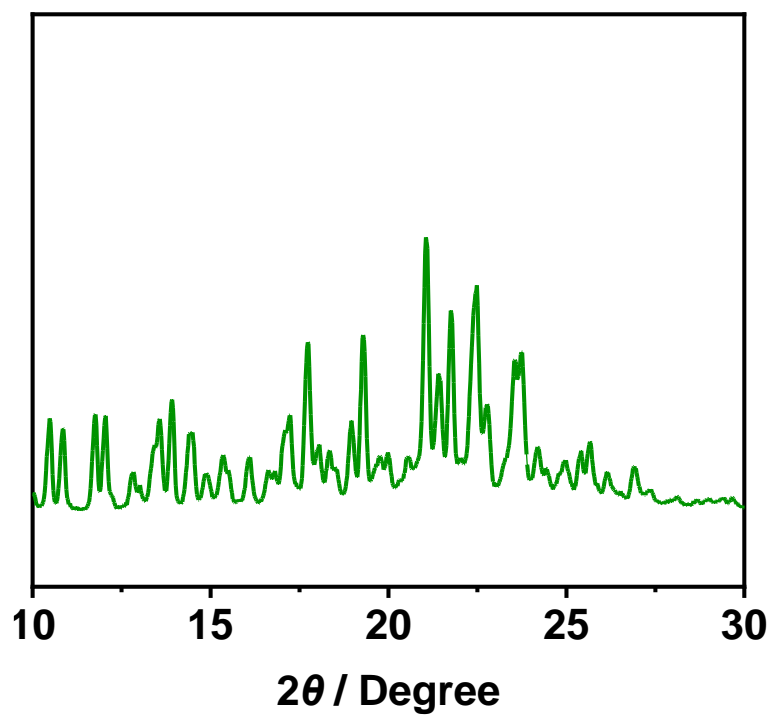


Fig. S15 Powder X-ray diffraction pattern of **PrP5 α** after being exposed to **MC** vapor for 48 h.

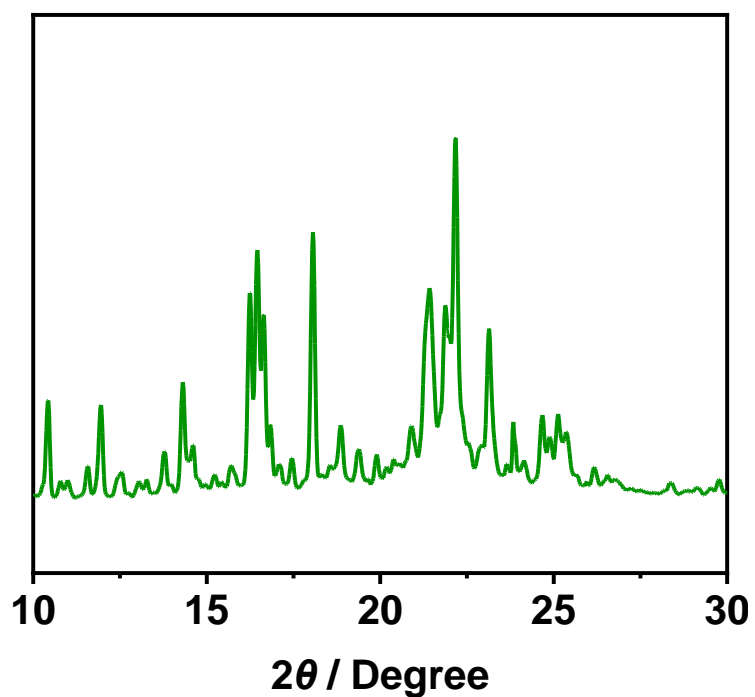


Fig. S16 Powder X-ray diffraction pattern of **PrP5 α** after being exposed to **PC** vapor for 48 h.

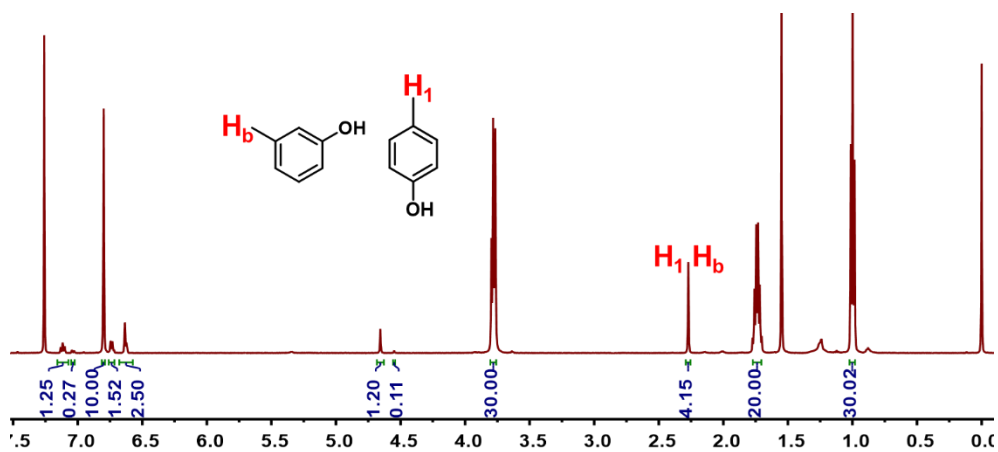


Fig. S17 ¹H NMR spectrum (400 MHz, CDCl₃, room temperature) of **PrP5α** after being exposed to the vapor of an equivolume mixture of **MC** and **PC** for 48 h.

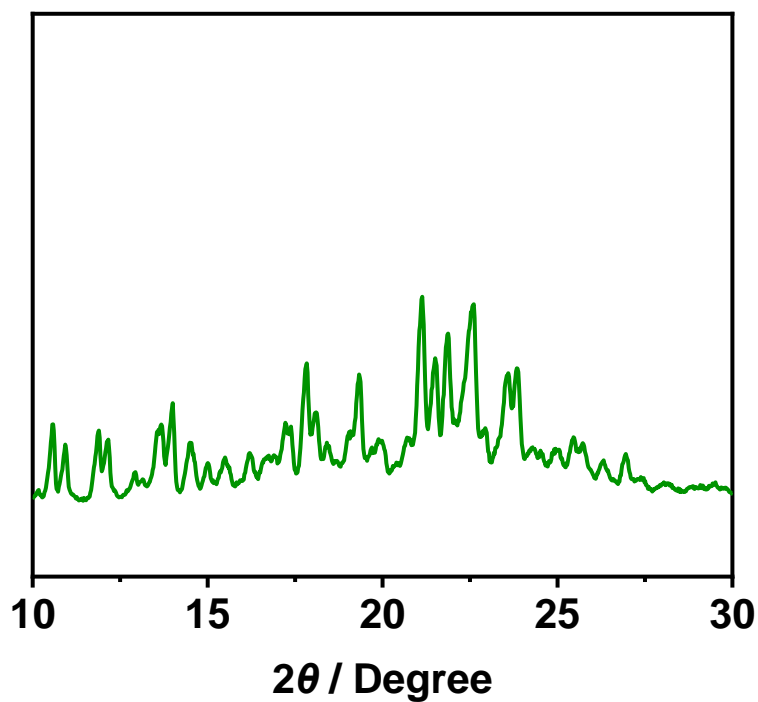


Fig. S18 Powder X-ray diffraction pattern of **PrP5α** after being exposed to the vapor of an equivolume mixture of **PC** and **MC** for 48 h.

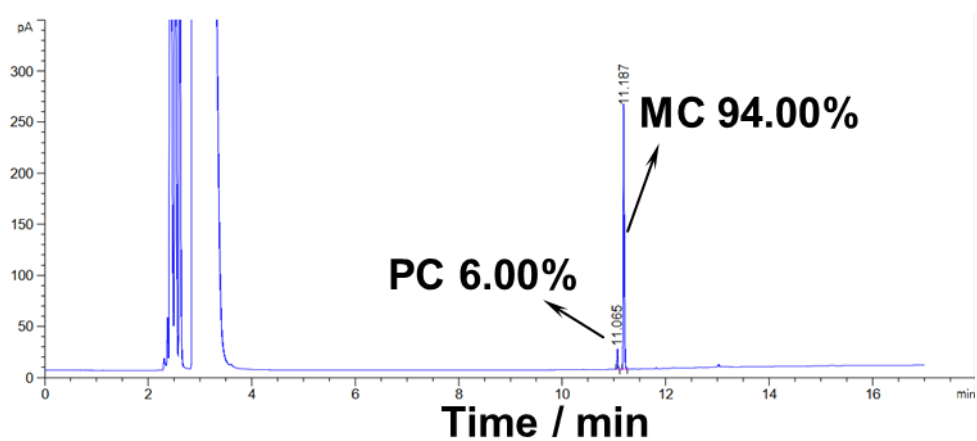


Fig. S19 The GC spectrum of relative uptake of MC and PC adsorbed in PrP5 crystals over 48 h using GC.

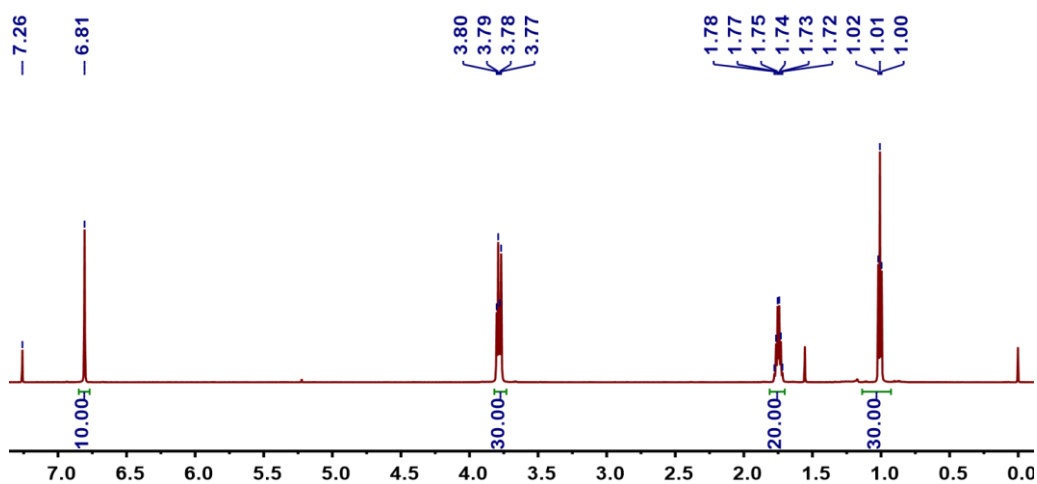


Fig. S20 ¹H NMR spectrum (500 MHz, CDCl₃, room temperature) of PrP5 after desorption.

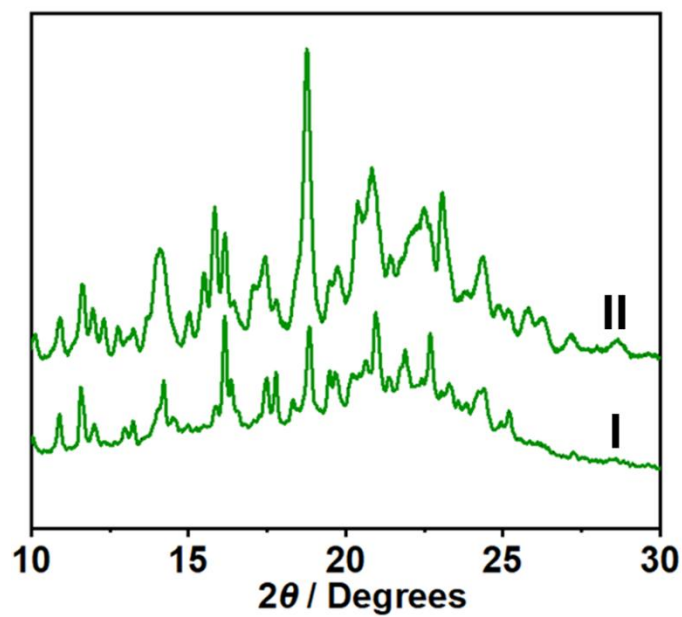


Fig. S21 PXR D patterns of **PrP5 α** : (I) after desorption under vacuum; (II) original **PrP5 α** .

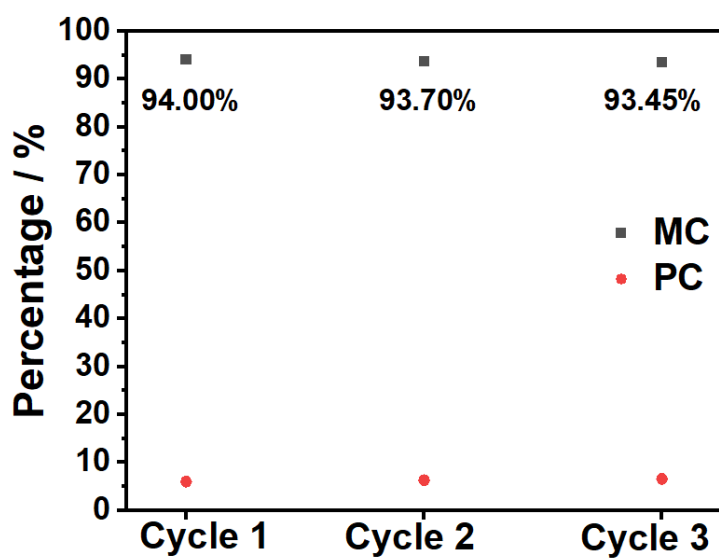


Fig. S22 The selectivity of **MC** uptake by **PrP5** over three cycles.

7. Studies of selective adsorption behavior of **EtP5** and **BuP5** solids

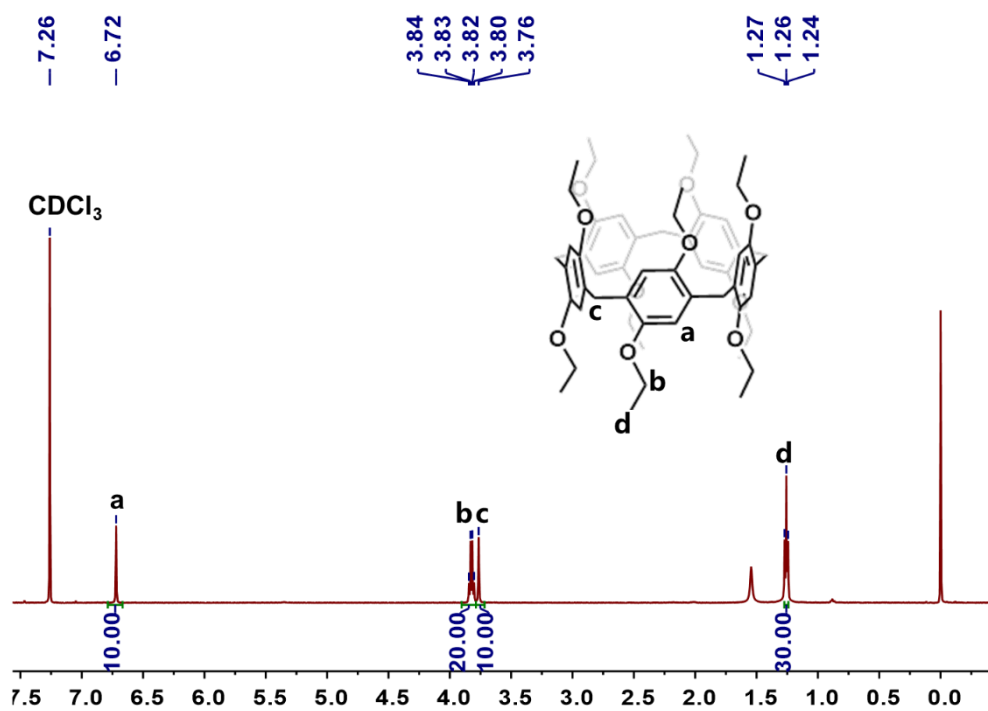


Fig. S23 ¹H NMR spectrum (500 MHz, CDCl₃, room temperature) of **EtP5**.

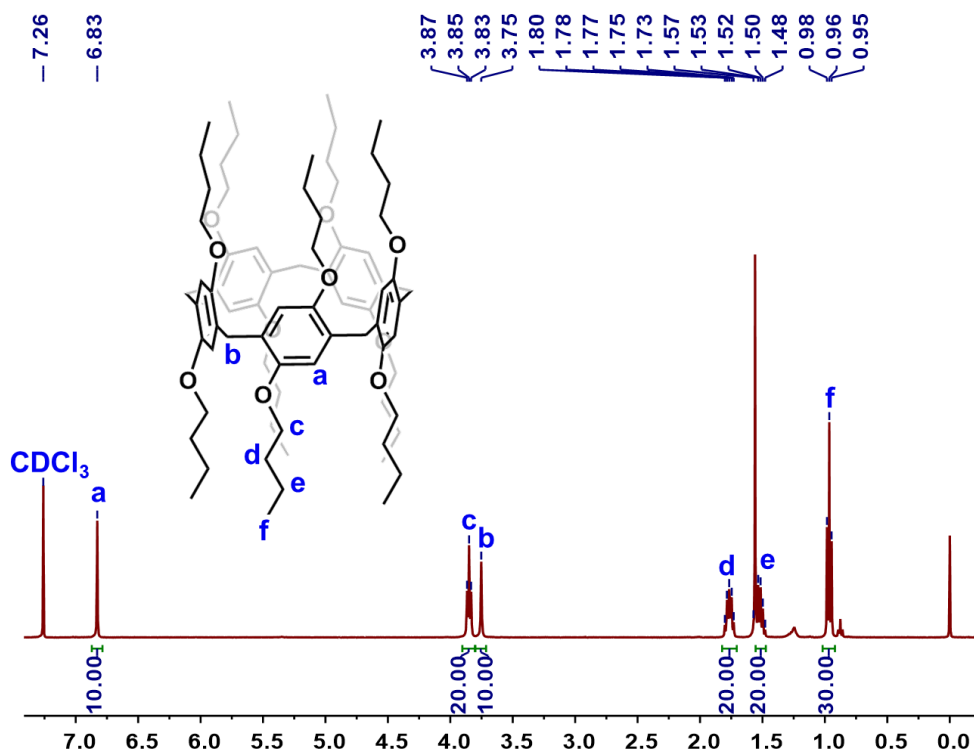


Fig. S24 ¹H NMR spectrum (500 MHz, CDCl₃, room temperature) of **BuP5**.

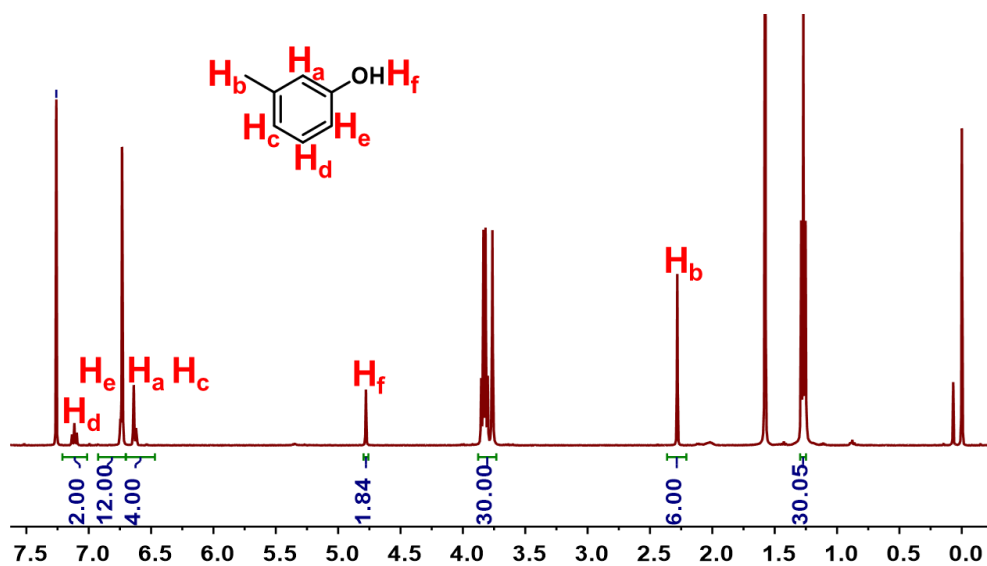


Fig. S25 ^1H NMR spectrum (400 MHz, CDCl_3 , room temperature) of guest-free **EtP5** crystals after being exposed to **MC** vapor for 48 h. Quantitative analysis of the NMR peak integrals revealed an adsorption stoichiometry of ~ 2.00 equivalents of **MC** per **EtP5** molecule.

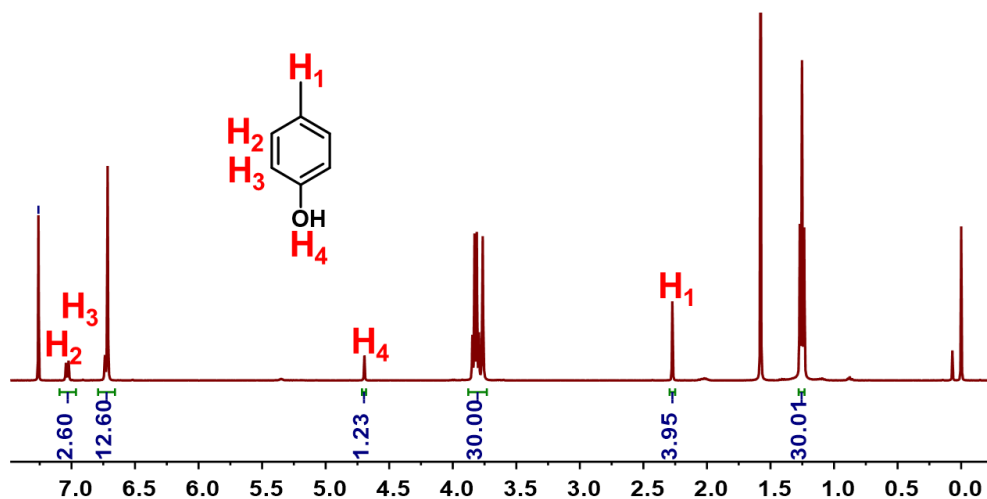


Fig. S26 ^1H NMR spectrum (400 MHz, CDCl_3 , room temperature) of guest-free **EtP5** crystals after being exposed to **PC** vapor for 48 h. Quantitative analysis of the NMR peak integrals revealed an adsorption stoichiometry of ~ 1.30 equivalents of **PC** per **EtP5** molecule.

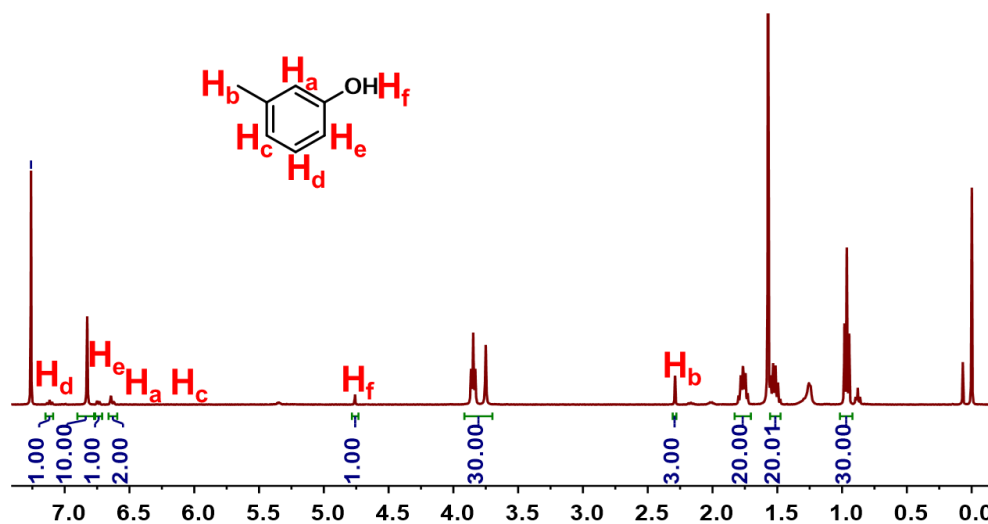


Fig. S27 ^1H NMR spectrum (400 MHz, CDCl_3 , room temperature) of guest-free **BuP5** crystals after being exposed to **MC** vapor for 48 h. Quantitative analysis of the NMR peak integrals revealed an adsorption stoichiometry of ~ 1.00 equivalent of **MC** per **BuP5** molecule.

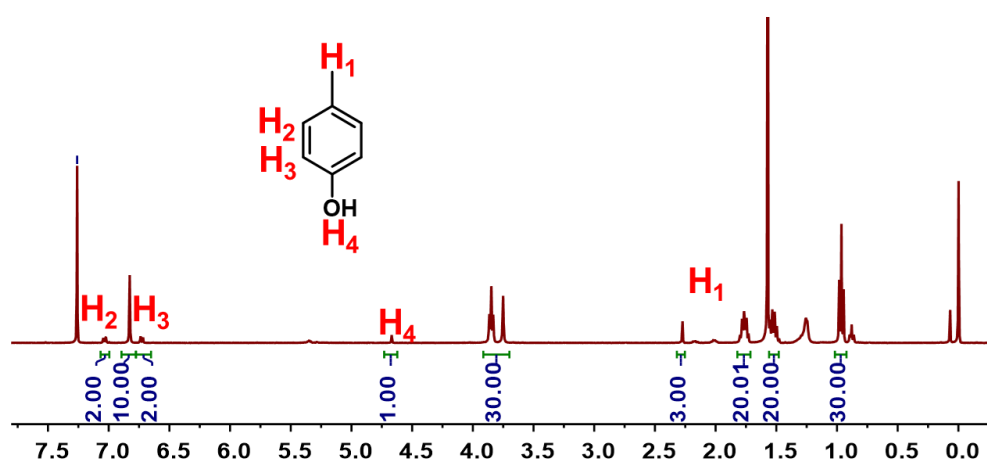


Fig. S28 ^1H NMR spectrum (400 MHz, CDCl_3 , room temperature) of guest-free **BuP5** crystals after being exposed to **PC** vapor for 48 h. Quantitative analysis of the NMR peak integrals revealed an adsorption stoichiometry of ~ 1.00 equivalent of **PC** per **BuP5** molecule.

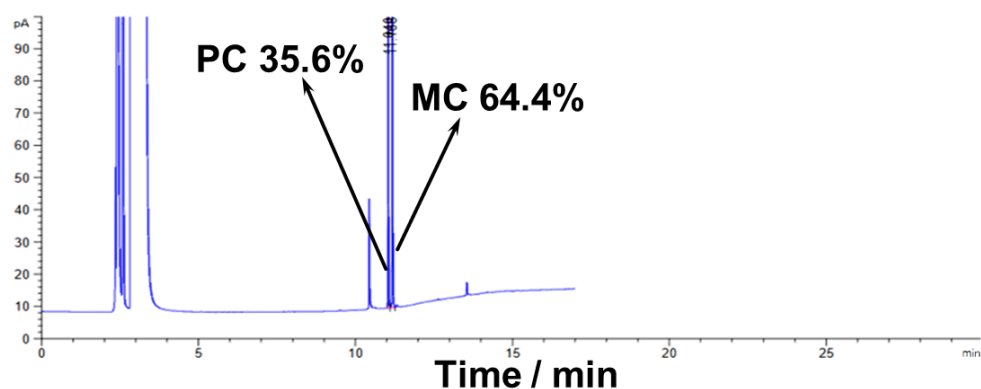


Fig. S29 The relative uptake of MC and PC adsorbed in **EtP5** crystals over 48 h in the competitive adsorption experiment.

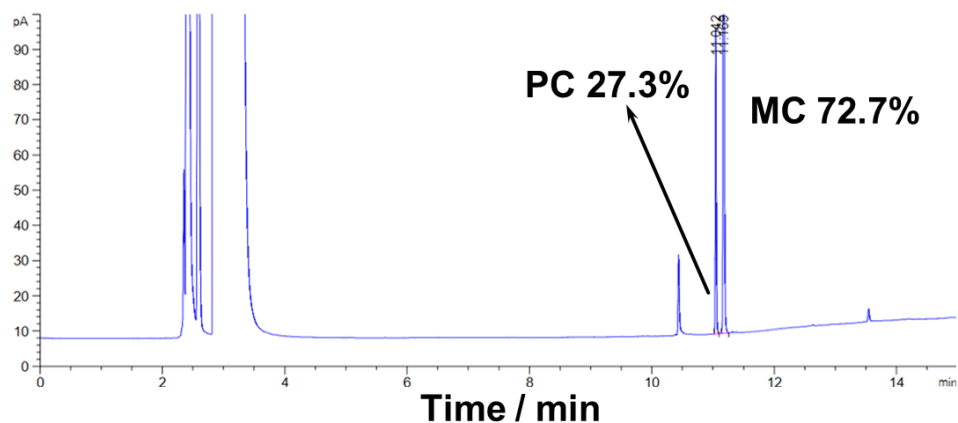


Fig. S30 The relative uptake of MC and PC adsorbed in **BuP5** crystals over 48 h in the competitive adsorption experiment.

8. Studies of selective adsorption behavior of **PrP5@MSN-OH** solids



Fig. S31 MSN-OH synthesized according to established protocols.^{S10}

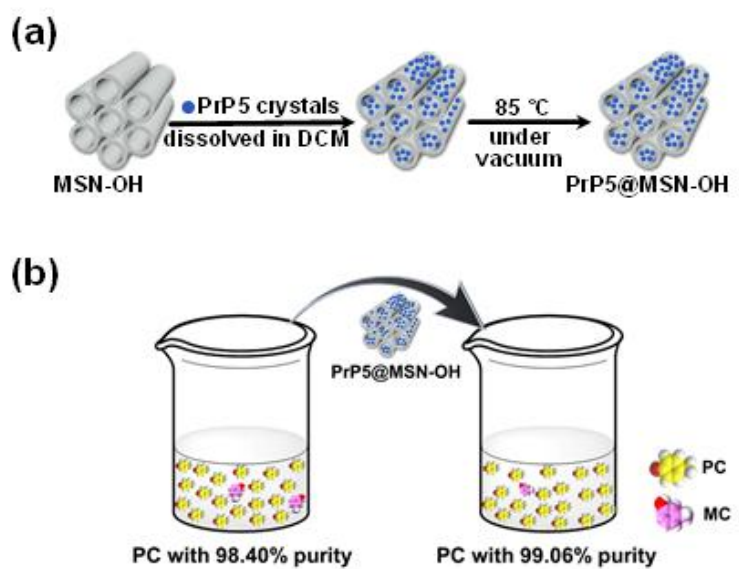


Fig. S32 Schematic illustrations: (a) the preparation of **PrP5@MSN-OH**; (b) the fine purification of **PC**.

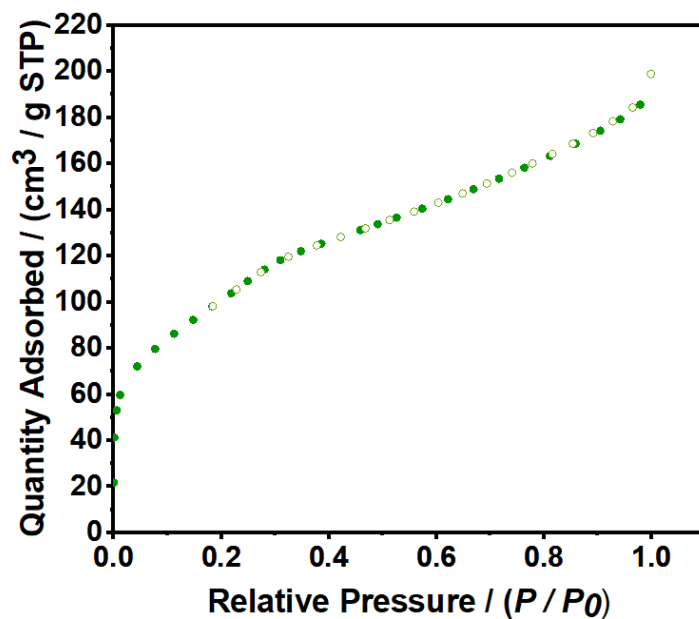


Fig. S33 N₂ adsorption isotherm of PrP5@MSN-OH. The BET surface area value is 370 m² g⁻¹. Adsorption, solid symbols; desorption, open symbols.

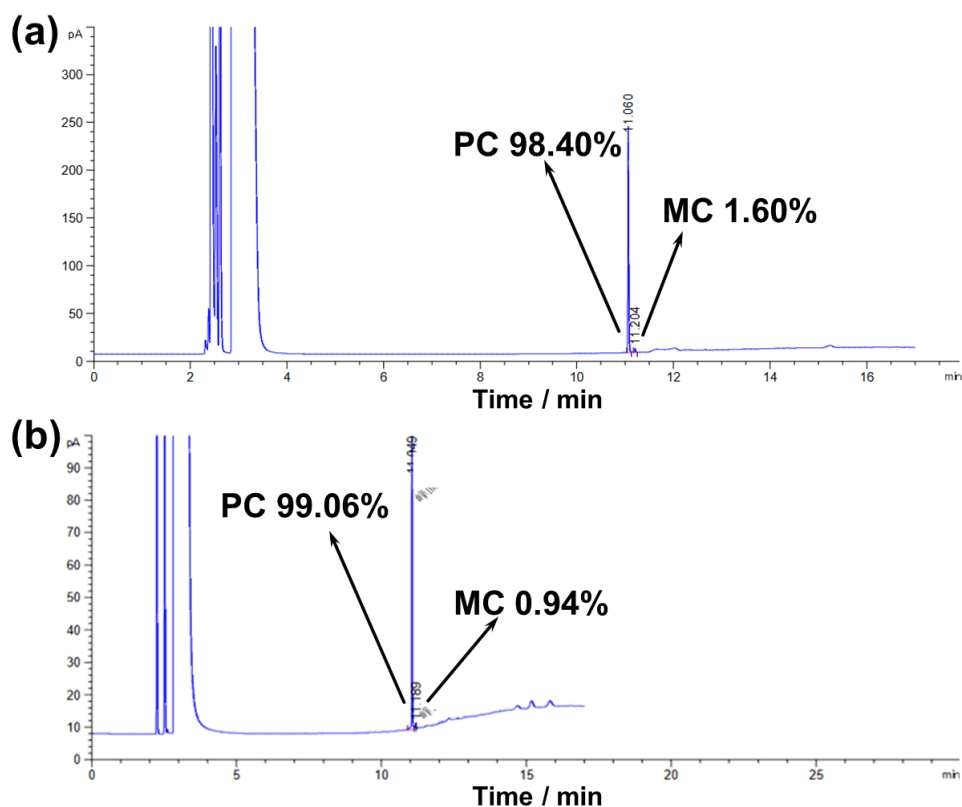


Fig. S34 Purification of a high-purity PC solution containing trace amounts of MC using PrP5-modified MSN-OH: (a) before purification; (b) after purification.

9. References

- S1. T. Ogoshi, S. Kanai, S. Fujinami, T. Yamagishi and Y. Nakamoto, *para*-Bridged symmetrical pillar[5]arenes: Their lewis acid catalyzed synthesis and host–guest property, *J. Am. Chem. Soc.*, 2008, **130**, 5022.
- S2. T. Ogoshi, T. Yamagishi and Y. Nakamoto, Pillar-shaped macrocyclic hosts pillar[n]arenes: New key players for supramolecular chemistry, *Chem. Rev.*, 2016, **116**, 7937.
- S3. F. Neese, Software update: the ORCA program system, version 4.0, *WIREs Comput. Mol. Sci.*, 2018, **8**, e1327.
- S4. A. D. Becke, Density-functional thermochemistry. III. The role of exact exchange, *J. Chem. Phys.*, 1993, **98**, 5648–5652.
- S5. P. C. Hariharan and J. A. Pople, The influence of polarization functions on molecular orbital hydrogenation energies, *Theor. Chim. Acc.*, 1973, **28**, 213–222.
- S6. S. Grimme, S. Ehrlich and L. Goerigk, Effect of the damping function in dispersion corrected density functional theory, *J. Comput. Chem.*, 2011, **32**, 1456–1465.
- S7. T. Lu and Q. Chen, Independent gradient model based on Hirshfeld partition: A new method for visual study of interactions in chemical systems, *J. Comput. Chem.*, 2022, **43**, 539–555.
- S8. T. Lu and F. Chen, Multiwfn: A multifunctional wavefunction analyzer, *J. Comput. Chem.* 2012, **33**, 580–592.
- S9. W. Humphrey, A. Dalke and K. Schulten, VMD: Visual molecular dynamics, *J. Mol. Graph.*, 1996, **14**, 33–38.
- S10. Y.-L. Sun, Y. Zhou, Q.-L. Li and Y.-W. Yang, Enzyme-responsive supramolecular nanovalves crafted by mesoporous silica nanoparticles and choline-sulfonatocalix[4]arene [2]pseudorotaxanes for controlled cargo release, *Chem. Commun.*, 2013, **49**, 9033–9035.